Journal of Materials Science: Materials in Electronics (2019) 30:8537–8545
https://doi.org/10.1007/s10854-019-01174-7

One-pot hydrothermal synthesis of $MoSe_2$ nanosheets spheres-reduced graphene oxide composites and application for high-performance supercapacitor

Zhao Wang[1] · Hong Yan Yue[1] · Ze Min Yu[1] · Fei Yao[2] · Xin Gao[1] · En Hao Guan[1] · Hong Jie Zhang[1] · Wan Qiu Wang[1] · Shan Shan Song[1]

Received: 25 September 2018 / Accepted: 19 March 2019 / Published online: 1 April 2019

Abstract
$MoSe_2$ nanosheets spheres ($MoSe_2$·NSs) were synthesized directly on the surface of reduced graphene oxide (rGO) nanosheets ($MoSe_2$–rGO) using a simple one-pot hydrothermal approach, which was used for supercapacitor. The synergistic effect of the $MoSe_2$·NSs and the highly conductive rGO network endows the $MoSe_2$–rGO composite excellent electrochemical performance. The effect of the content of graphene in the composite were investigated in details. The optimal electrode exhibits a high specific capacitance of 814.4 F g^{-1} at 1 A g^{-1} in 2 M KOH. Moreover, the assembled supercapacitor delivers a high specific capacitance of 215.7 F g^{-1} at 1 A g^{-1} and retains 81.7% of the initial capacitance at 10 A g^{-1} after 5000 cycles. It suggests that it has potential as an electrode material for high-performance electrochemical supercapacitors.

1 Introduction

Supercapacitor, also called electrochemical supercapacitor, is a promising energy storage equipment between conventional capacitors and batteries, which exhibits high power density, good cyclic stability, and excellent reversibility [1, 2]. Supercapacitor can be divided into two basic types due to the different charge storage mechanisms: electrical double-layer capacitors (EDLCs) and pseudocapacitors. The former stores charge by charge separation at the electrode–electrolyte interface and the latter is mainly attributed to a fast Faraday reaction [3–5]. Pseudocapacitors have a higher specific capacitance than EDLC, but its specific capacitance tends to gradually decrease due to poor electrical conductivity. It has become a major research subject to synthesize materials which can simultaneously apply these two mechanisms [6–8].

Transition metal dichalcogenides (TMDC) become an ideal choice for advanced electrode materials of supercapacitor owing to their 2D sheet-like morphology, large surface area and diverse material property [9–12]. TMDC compounds with a general formula MX_2 (M: Mo or W, X: S or Se), are subjected to strong covalent bonds (X–M–X), whereas the individual layers are stacked together by weak van der Waals interactions [13–15]. Among them, $MoSe_2$, an semiconductor with a band gap of ~ 1.5 eV, has high theoretical capacity and low cost, which has been investigated and is considered as one of the attractive materials for supercapacitor electrode materials [16–18]. Similar to that of other metal oxides, its specific capacitance decline significantly with the increase of scanning rate as a result of the poor conductivity [19].

Graphene, an atomic sheet of sp^2-hybrided carbon atoms, has a large specific surface area, high conductivity and ultra-high chemical stability [20–23]. Currently, the preparation method of graphene mainly includes reduction of graphene oxide (GO) and chemical vapor deposition. Chemical reduction of GO to reduced GO (rGO) has the characteristics of large-scale preparation and low cost, which has attracted people's attention [24]. In addition, the surface of RGO has oxygen-containing functional groups, resulting in its good hydrophilicity and facile to be modified to produce graphene

Electronic supplementary material The online version of this article (https://doi.org/10.1007/s10854-019-01174-7) contains supplementary material, which is available to authorized users.

✉ Hong Yan Yue
hyyue@hrbust.edu.cn

[1] School of Materials Science and Engineering, Harbin University of Science and Technology, Harbin 150040, People's Republic of China

[2] Department of Materials Design and Innovation, University at Buffalo, North Campus, Buffalo 14260, USA

matrix composites [25]. Graphene exhibits a superior stability, but the capacitance is relatively low due to the mechanism of EDLCs [26, 27]. The combination of graphene and $MoSe_2$ can increase not only the electrical conductivy but also give full play to pseudocapacitance of the $MoSe_2$ and double-layer capacitance characteristics of the graphene.

Some researches based on $MoSe_2$ material for supercapacitor have been reported in recent years. Juns et al. synthesized $MoSe_2$ nanosheets and measured it in the 1 M H_2SO_4, which showed a specific capacity of 30 F g^{-1} at 1 A g^{-1} [16]. Gao et al. reported the $MoSe_2$ spheres prepared by hydrothermal sythesis, which demonstrated a specific capacitance of 243 F g^{-1} at 0.5 A g^{-1} in the 2 M KOH [17]. Karade and Sankapal reported the $MoSe_2$/MWCNTs hybrid for supercapacitor electrode, which showed a specific capacitance of 232 F g^{-1} at 1.4 A g^{-1} [18]. Huang et al. synthesized layered $MoSe_2$ nanosheets on Ni-foam via a hydrothermal method and it exhibited a specific capacitance of 1114.3 F g^{-1} at 1 A g^{-1} [28]. Balasingam et al. prepared $MoSe_2$/rGO nanosheet for supercapacitor electrode and showed a specific capacitance of 211 F g^{-1} at a scan rate of 5 mV s^{-1}. However, when the scan rate of 125 mV s^{-1}, its specific capacitance drops rapidly to 100 F g^{-1} [29]. This paper only compared the electrochemical properties of $MoSe_2$/rGO and pure $MoSe_2$. The influence of graphene content on the performance of supercapacitors was not investigated in details. However, it is necessary to explore the influence of graphene content on the electrochemical performance of composites for supercapacitors.

Herein, the $MoSe_2$ nanosheet spheres ($MoSe_2$·NSs)–rGO composite were synthesized by a facile one-pot hydrothermal approach. The $MoSe_2$–rGO composite reveals a synergistic effect, which results in the enhanced performance. The optimal electrochemical performance (814.4 F g^{-1} at 1 A g^{-1}) is achieved in the $MoSe_2$–rGO-25 composite. Moreover, the assembled supercapacitor based on $MoSe_2$–rGO-25 composite also possesses a high specific capacitance of 215.7 F g^{-1} at 1 A g^{-1} and long cycle life with 81.7% capacitance retention after 5000 cycles at 10 A g^{-1}. It can be applied as a promising supercapacitor electrode.

2 Experimental

2.1 Chemical and reagents

Graphite powders were supplied by Sigma Aldrich. Poly(tetrafluoroethylene) binder (PTFE), Nickel foam and carbon black was purchased from Macklin reagent. Se powders, Na_2MoO_4 and N_2H_4·H_2O were brought from Tianjin Guangfu Fine Chemical Research Institute (China). $KMnO_4$, KOH, H_2O_2 (30 wt%), HCl (36 wt%), H_2SO_4 (98 wt%) and ethanol were brought from Tianli Chemical Reagent Co., Ltd (China). Spring gasket, stainless steel gasket, separator and LIR 2016 coin cell case were purchased from Shenzhen Tiancheng Technology Co., Ltd (China).

2.2 Preparation of $MoSe_2$–rGO composites

Figure 1 shows the schematic of the synthesis of $MoSe_2$–rGO nanocomposite for supercapacitor. GO was synthesized by a modified Hummers' method using natural graphite powders as the raw material, which is similar to the previous report [30]. Firstly, 25 mg GO was first ultrasonically dispersed in 65 mL distilled water to form a suspension. 2 mmol Na_2MoO_4 was added into the GO suspension. At the same time, 4 mmol Se powders were dissolved in 10 mL N_2H_4·H_2O under the constant magnetic stirring in a separate beaker. The hydrate–Se solution was also slowly poured into the above GO suspension (Fig. 1a). Then, the mixture was transferred into a 100 mL Teflon-lined stainless steel autoclave and maintained at 200 °C for 12 h (Fig. 1b). The black precipitates were collected and washed by DI water and ethanol for three times. The final product ($MoSe_2$–rGO-25) was obtained after freeze-drying (Fig. 1c). The GO was reduced into rGO in this process and $MoSe_2$ NSs are grown on the surface of the rGO via the in-situ reduction of the MoO_4^{2-} and Se powders by N_2H_4·H_2O. In order to investigate the effect of graphene content on the electrochemical properties, GO with 15, 35, 50, 100 mg was also selected to combine with 2 mmol Na_2MoO_4 and 4 mmol Se powders, and the as-prepared sample was marked as $MoSe_2$–rGO-15, $MoSe_2$–rGO-35, $MoSe_2$–rGO-50, $MoSe_2$–rGO-100, respectively. Meanwhile, the pure $MoSe_2$ and rGO were also prepared under the same condition.

2.3 Characterizations

The morphologies of the $MoSe_2$, rGO and $MoSe_2$–rGO were acquired by a scanning electron microscope (SEM) (JSM7000F, JEOL). The X-ray diffraction (XRD) was conducted on a Rigaku Rotaflex D/MAX diffractometer using the Cu Kα radiation.

2.4 Eletrochemical measurements

All electrochemical measurements were achieved in a standard three-electrode system on a VMP3 electrochemical analyzer (France) at room temperature. As-prepared active materials, carbon black and PTFE were mixed in a mass ratio of 80:10:10 to obtain a viscous slurry and coated onto the nickle foam current collector (1 × 1 cm). The prepared active material loaded on the electrode was around 5 mg per electrode. The nickel foam wrapped in slurry was dried at 80 °C. Subsequently, the dried nickel foams were pressed into a thin foil and used as the

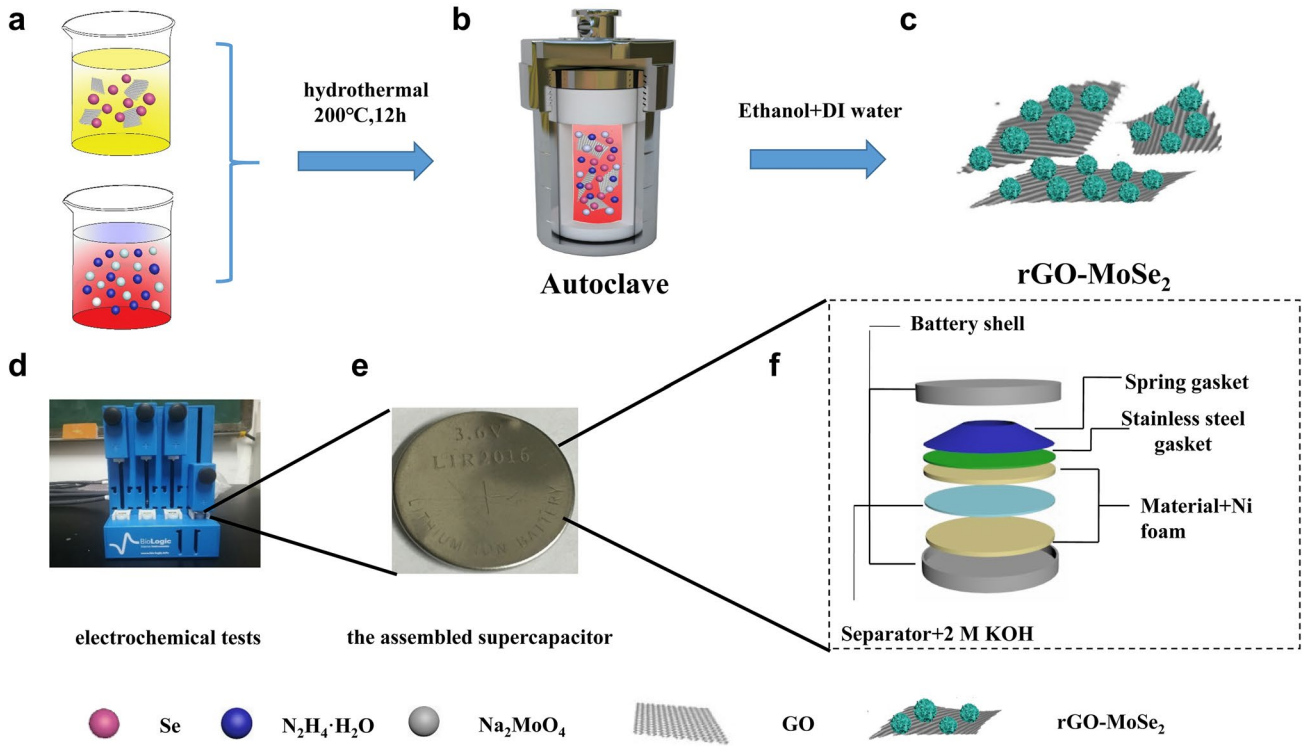

Fig. 1 Schematic of fabrication process of the $MoSe_2$–rGO nanocomposite for supercapacitor

working electrode. The reference and counter electrode were composed by an Ag/AgCl (3.0 M KCl) and a platinum foil electrode, respectively. The electrolyte used was 2 M KOH. In addition, the symetric supercapacitor was prepared with two electrodes, electrolyte, spring gasket, stainless steel gasket and separator in the LIR2016 coin cell. The coin cell was crimped using hydraulic cell crimping machine (MSK-110, China). Photograph of the electrochemical tests and the assembled supercapacitor are shown in Fig. 1d, e. The internal construction schematic of the assembled supercapacitor is shown in Fig. 1f. Electrochemical impedance spectroscopy (EIS) was obtained in the frequency range from 10 mHz to 100 kHz at open circuit potential with an ac perturbation of 5 mV. Cyclic voltametry (CV) responses were recorded at various scan rates of 10 to 100 mV s^{-1} from − 0.2 to 0.8 V. Galvanostatic charge discharge (GCD) curves were measured from 0 to 0.5 V at current densities of 1, 2, 4, 6, 8, 10 A g^{-1}. The discharge capacitance (C) of the asprepared electrode was calculated based on the following formula [31]:

$$C = \frac{I\Delta t}{m\Delta V} \tag{1}$$

where, I is the current (A), Δt denotes the discharging time (s), m is the weight of active materials (g), ΔV is the potential change in the discharge process.

The energy density (E) and power density (P) of the assembled supercapacitor according to the following equations [32]:

$$E = \frac{1}{2}C(\Delta V)^2 \tag{2}$$

$$P = \frac{E}{\Delta t} \tag{3}$$

where, C is the capacitance of the assembled supercapacitor, ΔV is the potential range and Δt is the discharge time.

3 Results and discussion

3.1 Characterizations of the $MoSe_2$–rGO nanocomposite

The SEM images and structures of the $MoSe_2$, rGO and $MoSe_2$–rGO nanocomposite are displayed in Fig. 2. It can be clearly observed that the pure $MoSe_2$ is composed of interlaced nanosheet spheres and they seriously agglomerate together (Fig. 2a). $MeSe_2$·NSs are densely dispersed on the surface of rGO network when the content of rGO nanosheets is smaller for $MoSe_2$–rGO-15 (Fig. 2b). With the increase of rGO content, $MeSe_2$·NSs are almost uniformly dispersed on the surface

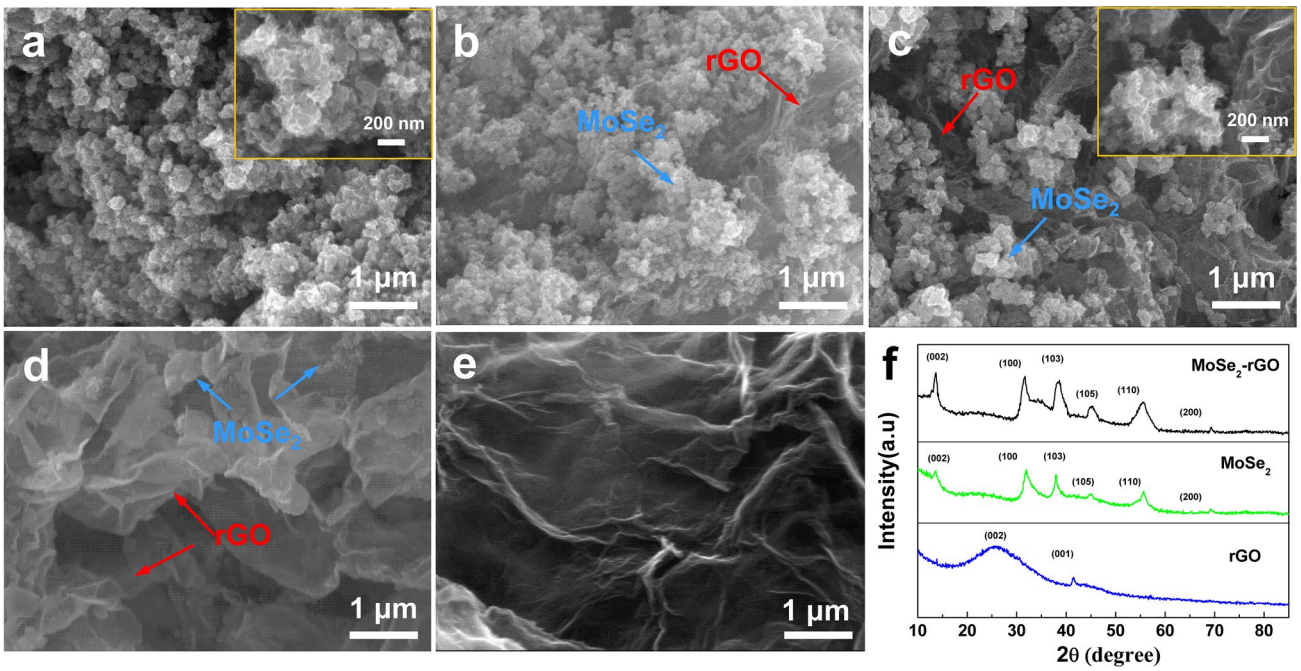

Fig. 2 SEM images and structures of the $MoSe_2$, rGO and $MoSe_2$–rGO nanocomposite. **a** SEM image of the $MoSe_2$. Inset: magnified image of $MoSe_2$. **b** SEM image of the $MoSe_2$–rGO-15. **c** SEM image of $MoSe_2$–rGO-25. Inset: magnified image of $MoSe_2$–rGO-25. **d** SEM image of the $MoSe_2$–rGO-100. **e** SEM image of the rGO. **f** XRD patterns of the $MoSe_2$, rGO and $MoSe_2$–rGO nanocomposite

of rGO nanosheets, as shown in $MoSe_2$–rGO-25 (Fig. 2c). The magnified image of $MoSe_2$–rGO-25 reveals that $MoSe_2$ and rGO are tightly integrated. When the rGO content continues to increase, $MoSe_2$ NSs are sparsely interspersed on the surface of rGO nanosheets, as shown in $MoSe_2$–rGO-100 (Fig. 2d). The rGO nanosheets exist in wrinkle shape, as shown in Fig. 2e. Figure 2f shows the XRD patterns of rGO, $MoSe_2$ and $MoSe_2$–rGO. The diffraction peaks of rGO at 26.3° and 41.5° represent the (002) and (001) reflections of graphene (JCPDS 75-1621), respectively. The diffraction peak of $MoSe_2$ at 13.2°, 31.8°, 37.9°, 44.8°, 55.6° and 69.2° corresponds to the (002), (100), (103), (105), (110) and (200) plane of $MoSe_2$, respectively (JCPDS: 77-1715) [33]. The intensity of the (002) plane peak of $MoSe_2$ is weaker than that of the $MoSe_2$–rGO, indicating that $MoSe_2$·NSs are full of rGO network.

The electrochemical behavior of the $MoSe_2$–rGO electrode was characterized in a typical three-electrode system. Figure 3a shows the CV curves of the electrodes with different rGO contents at a scan rate of 20 mV s^{-1} in 2 M KOH. The CV curve shows the presence of redox peaks, which might be occurred due to the electrochemical insertion/extraction of K^+ ions in the interlayer of layered $MoSe_2$·NSs. According to previous reports, the reaction may be accompanied by the faradaic and non-faradaic processes of the $MoSe_2$ [18].

$$(MoSe_2)_{suface} + K^+ + e^- \leftrightarrow (MoSe_2 - K)_{suface} \quad (4)$$

$$MoSe_2 + K^+ + e^- \leftrightarrow K - MoSe_2 \quad (5)$$

The area under the CV curve of $MoSe_2$–rGO-25 is obviously larger than that of other materials. This demonstrates that the $MoSe_2$-rGO-25 electrode has higher capacitance than that of the other electrode. Figure 3b shows the GCD curves of various electrode materials at a current density of 1 A g^{-1}. The $MoSe_2$–rGO-25 electrode shows the largest discharging time. Based on the GCD curves, the specific capacitance is calculated using Eq. (1). The calculated specific capacitance of various electrodes at 1 A g^{-1} increases intially and later decreases with increasing the initial GO content (Fig. 3c). In the $MoSe_2$–rGO-25, it is the highest, which is consistent with the CV result. This can be attributed to the good combination of $MoSe_2$ and rGO, which promotes the diffusion of ions and electrons in the electrolyte solution. This indicates that the graphene content has a great effect on the specific capacitance of the nanocomposite. Moreover, the peak current increases with the increase of scan rate and the CV curves almost keep the same profiles, which suggests this material has an excellent reversibility during the redox reactions at electrode/electrolyte interfaces (Fig. 3d).

Figure 3e shows GCD curves of the $MoSe_2$–rGO-25 at various current densities. The $MoSe_2$–rGO-25 electrode shows the largest discharging time at 1 A g^{-1}. The discharge specific capacitance values are calculated to be 814.4, 635.8, 491.7, 451.3, 419.7 and 403.9 F g^{-1} at 1, 2, 4, 6, 8 and 10 A g^{-1}, respectively (Fig. 3f). It can be seen that with increasing the curent density, the discharge specific capacitance of the $MoSe_2$–rGO-25 electrode decreases. This may

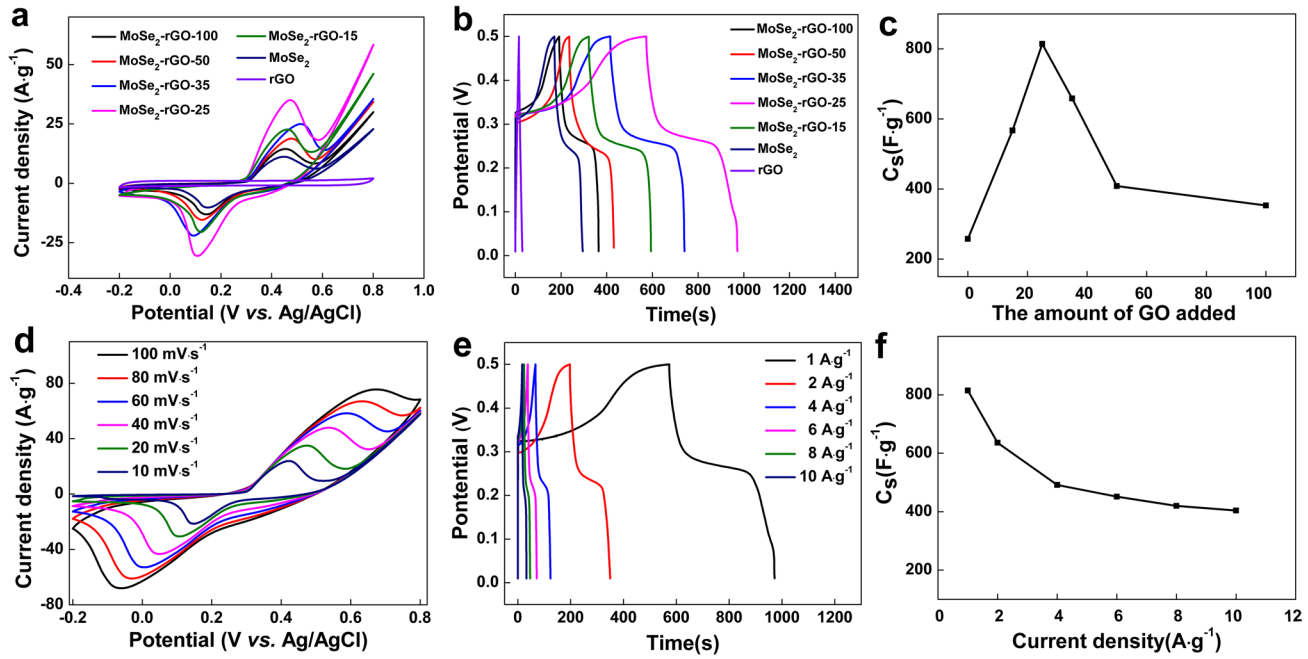

Fig. 3 Electrochemical performance of the $MoSe_2$–rGO nanocomposite. **a** CV curves of the different electrodes at a scan rate of 20 mV s^{-1}. **b** GCD curves of the different electrodes at 1 A g^{-1}. **c** Specific capacitances of the $MoSe_2$–rGO-25 electrode at 1 A g^{-1}. **d** CV curves of the $MoSe_2$–rGO-25 at different scan rates.**e** GCD curves of the $MoSe_2$–rGO-25 electrode at various current densities. **f** Specific capacitances of the $MoSe_2$–rGO-25 electrode at various current densities

be the insufficient Faradaic redox reactions of the active material at higher discharge current densities. Moreover, the CV and GCD curves of other as-prepared electrodes are shown in Fig. S1–S6, respectively. The shape of CV and GCD curves of other $MoSe_2$–rGO electrodes is consistent with the $MoSe_2$–rGO-25, but the specific capacity is lower than it (Fig. S1–S5). The CV curves of rGO electrode take roughly rectangular shapes and the GCD curves of rGO electrode present a typical triangular shapes, which indicates that the rGO electrode exhibits only double-layer capacitance characteristics (Fig. S6).

EIS analysis was used to study the resistive and capacitive behaviors of the electrode materials for supercapacitor. Figure 4 shows the Nyquist plots of rGO, $MoSe_2$ and various $MoSe_2$–rGO electrode. The slope of the curve of $MoSe_2$–rGO-25 in the low frequency region is between rGO and $MoSe_2$, which is slightly lower than that of pure rGO and higher than that of other $MoSe_2$–rGO electrodes, indicating

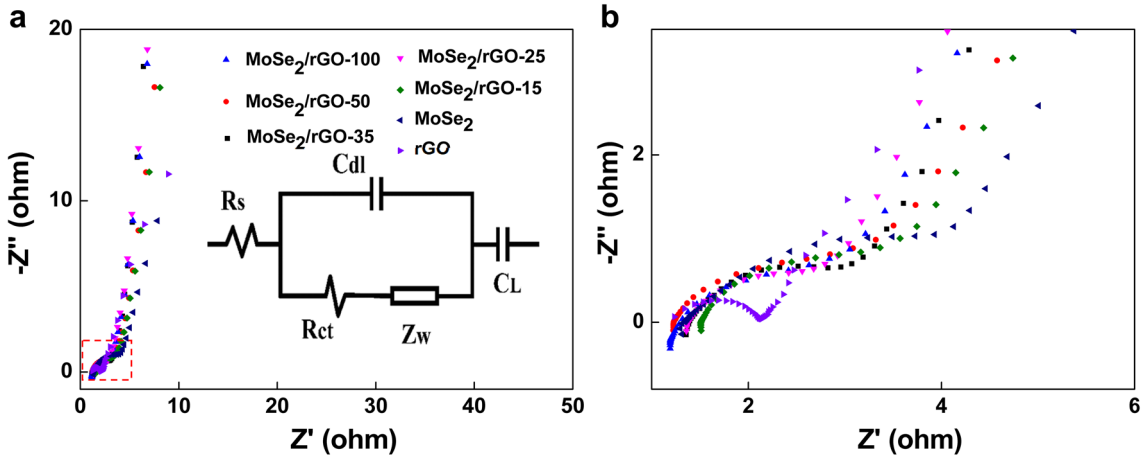

Fig. 4 Electrochemical performance. **a** Nyquist plots of various electrodes. Inset: the modeled equivalent circuit of EIS **b** the zoom-in Nyquist plots at the high-frequency region

that it has a good equivalent series resistance. The Nyquist plot is explained by the corresponding fitting equivalent circuit (inset of Fig. 4a), where Rs stands for the intrinsic ohmic resistance (comes from the intrinsic resistances of electrode material, electrolyte, current collector, leads and separator, as well as the contact resistances between them), which can be suggested by the first intercept along the real axis [34]. Rct is the interfacial charge transfer resistance (comes from the electronic and ionic resistances at the interface between the electrode and the electrolyte), which can be suggested by the diameter of the semicircle. This resistance mainly depends on the wettability between the electrolyte and electrode, the morphology and conductivity of electrode [35]. The Warburg diffusion resistance (Z_w) comes from the resistance for ion diffusion from electrolyte into the electrode, corresponding to the projected length of Warburg region on the real axis [36]. C_{dl} is the double layer capacitance and C_L is the Faradic capacitance [37]. The calculated Rct values for the rGO, $MoSe_2$, $MoSe_2$–rGO-15, $MoSe_2$–rGO-25, $MoSe_2$–rGO-35, $MoSe_2$–rGO-50 and $MoSe_2$–rGO-100 electrodes are 2.15, 4.06, 3.45, 2.71, 2.88, and 2.64 Ω, respectively, which indicates that the charge transfer performance can be effectively improved by combining $MoSe_2$ and rGO. The Rs values of the rGO, $MoSe_2$, $MoSe_2$–rGO-15, $MoSe_2$–rGO-25, $MoSe_2$–rGO-35, $MoSe_2$–rGO-50 and $MoSe_2$–rGO-100 electrodes are 1.23, 1.31, 1.51, 1.35, 1.24, 1.34 and 1.35 Ω, respectively (Fig. 4b). It is suggested that the active material of the electrode are in good contact with the collector and the electrolyte.

Figure 5 shows the specific discharge capacitances of the different electrodes at various current densities. The specific capacity decreases with increasing the current density and the $MoSe_2$–rGO-25 shows the largest specific capacitance. The improvement of electrochemical properties of the $MoSe_2$–rGO-25 is mainly attributed to the following reasons: (1) $MoSe_2$ NSs anchored on the rGO nanosheets provide more electroactive sites by EDLC as well as pseudocapacitance process; (2) rGO nanosheets effectively improve the electrical conductivity of the composite. (3) The addition of rGO effectively changes the dispersion of $MoSe_2$ NSs in the composite. The excessive content of $MoSe_2$ NSs or rGO hinders the diffusion of ions.

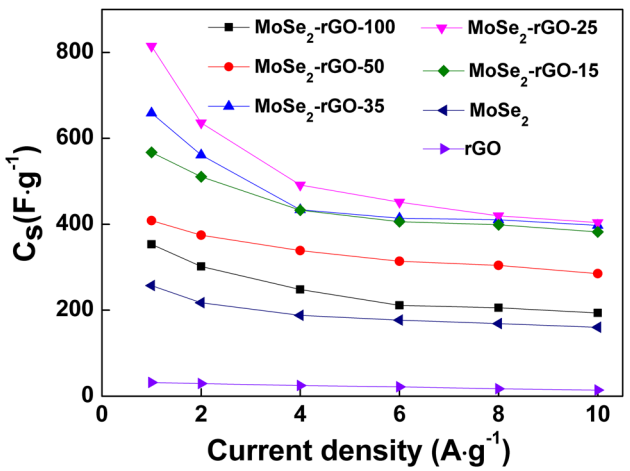

Fig. 5 Specific capacitances of the different electrodes at various current densities

Figure 6a show GCD curves of the assembled supercapacitor based on $MoSe_2$–rGO-25 at various current densities in 2 M KOH. The discharge specific capacitance values are calculated to be 215.7, 186.3, 182.4, 180.9, 173.3, 137.3 F g^{-1} at 1, 2, 4, 6, 8 and 10 A g^{-1} (Fig. 6b). A comparison of the specific capacity of the MoSe2–rGO-25 based supercapacitors with previous reports are summarized in Table 1 [38–45]. The cyclic stability of the assembled supercapacitor is evaluated using GCD analysis for 5000 cycles at 10 A g^{-1} and the specific capacitance of the assembled supercapacitor retains 81.7% (Fig. 6c). This maybe that the close bonding between the rGO and $MoSe_2$ effectively improves the long-term stability. The Ragone plot for the assembled supercapacitor is shown in Fig. 6d. The energy and power densities of the assembled supercapacitor were estimated according to Eqs. (2, 3), respectively. Our supercapacitor device exhibits maximum energy density of 6.9 Wh kg^{-1} at lower power density of 257.4 W kg^{-1} at 1 A g^{-1}. The energy density was 1.2 Wh kg^{-1} with a power density of 1127.6 W kg^{-1}. The superior performance of the supercapacitor shows a great potential in the practical application.

4 Conclusions

In summary, The $MoSe_2$–rGO nanocomposite were obtained for supercapacitor. First, GO was prepared by Hummers' method. Subsequently, GO was added into Na_2MoO_4 solution and hydrazine hydrate–Se in distilled water for the hydrothermal reaction. The GO was reduced into rGO in this process and $MoSe_2$ NSs are grown on the surface of the rGO. The effect of graphene content on the morphologies and electrochemical properties were investigated in details. The optimal electrode ($MoSe_2$–rGO-25) exhibites a high specific capacitance of 814.4 F g^{-1} at 1 A g^{-1}. The assembled supercapacitor based on $MoSe_2$–rGO-25 possesses a high specific capacitance of 215.7 at 1A g^{-1} and excellent cycle life with 81.7% capacitance retention after 5000 cycles at 10 A g^{-1}.

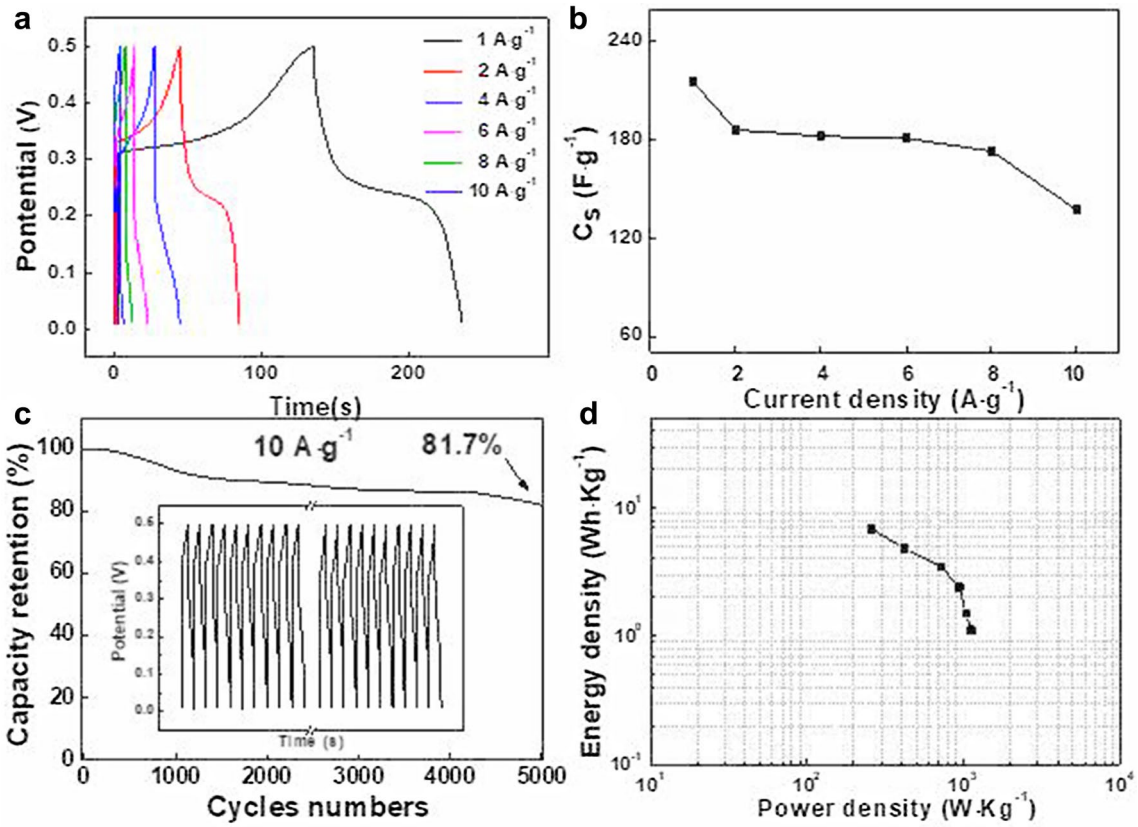

Fig. 6 Electrochemical performance of the the assembled supercapacitor. **a** GCD curves of the assembled supercapacitor at various current densities. **b** Specific capacitances of the assembled supercapacitor at various current densities. **c** Cycle test of the assembled supercapacitor with a GCD at a current density of 10 A g^{-1}. **d** Ragone plots related to energy and power densities of the assembled supercapacitor

Table 1 A comparison of the specific capacity for various materials based supercapacitors

Sample	Electrolyte	The specific capacity	References
PEDOT/rGO	6 M KOH	102.8 F g^{-1} at 10 mV s^{-1}	[38]
Nb_2O_5/rGO	1 M $LiClO_4$ in EC/PC	26.61 F g^{-1} at 1 mA cm^{-2}	[39]
	1 M $NaClO_4$ in EC/PC	41.28 F g^{-1} at 1 mA cm^{-2}	
PEDOT–PSS/GNPs	NH_4Tf/EMITf/PVdF-HFP	106 F g^{-1} at 0.5 mA cm^{-2}	[40]
MoS_2 films	1.0 M LiOH	7.8 mC cm^{-2} at 1 mA cm^{-2}	[41]
		6.8 mC cm^{-2} at 50 mV s^{-1}	
$CuMnO_2$	6 M KOH	272 F g^{-1} at 0.5 A g^{-1}	[42]
NiSe@$MoSe_2$/N-PMCN	2 M KOH	223 F g^{-1} at 1 A g^{-1}	[43]
$NiCo_2S_4$@HGH	3 M KOH	312.6 F g^{-1} at 6 A g^{-1}	[44]
PANI/(MnO_2–RGO)/PANI	6 M KOH	148 F g^{-1} at 1 A g^{-1}	[45]
MoO_3/GF aerogel		105 F g^{-1} at 1 A g^{-1}	
$MoSe_2$–RGO	2 M KOH	215.7 F g^{-1} at 1 A g^{-1}	Ours

PEDOT/rGO poly(3,4-ethylenedioxythiopene)/ reduced grapheneoxide, *PEDOT-PSS/GNPs* poly(3,4-ethylenedioxythiophene)-poly(styrenesulfonate)/graphene nano-platelets, *EC/PC* ethylene carbonate / propylene carbonate (1:1by volume), *NH_4Tf/EMITf/PVdF-HFP* Ammonium trifluoromethanesulfonate/1-ethyl-3-methylimidazolium trifluoromethanesulfonate/poly(vinylidine fluoride-co-hexafluoropropylene), *NiSe@$MoSe_2$/N-PMCN* NiSe@$MoSe_2$ nanosheet arrays/the nitrogen-doped pomelo mesocarps-based carbon nanosheet, *$NiCo_2S_4$@HGH* Nickel cobalt sulfide nanoparticles embedded in holey defect graphene hydrogel, *PANI/(MnO_2-RGO)/PANI* sandwich-type PANI decorated 3D porous manganese dioxide/reduced GO hybrid film, *MoO_3/GF aerogel* 3D molybdenum oxide/graphene aerogel

Acknowledgements This work is supported by the fundamental research foundation for University of Heilongjiang province (Grant No. LGYC2018JQ012), the Innovative Talent Fund of Harbin city (Grant No. 2016RAQXJ185).

References

1. J.-H. Choi, C. Lee, S. Cho, G. Moon, B.-S. Kim, H. Chang, H.D. Jang, High capacitance and energy density supercapacitor based on biomass-derived activated carbons with reduced graphene oxide binder. Carbon **132**, 16–24 (2018). https://doi.org/10.1016/j.carbon.2018.01.105
2. M. Liu, Z. Wang, J. Liu, G. Wei, J. Du, Y. Li, C. An, J. Zhang, Synthesis of few-layer 1T′-$MoTe_2$ ultrathin nanosheets for high-performance pseudocapacitors. J. Mater. Chem. A **5**, 1035–1042 (2017). https://doi.org/10.1039/c6ta08206h
3. V.K. Mariappan, K. Krishnamoorthy, P. Pazhamalai, S. Sahoo, S.J. Kim, Electrodeposited molybdenum selenide sheets on nickel foam as a binder-free electrode for supercapacitor application. Electrochim. Acta **265**, 514–522 (2018). https://doi.org/10.1016/j.electacta.2018.01.075
4. W. Yang, L. He, X. Tian, M. Yan, H. Yuan, X. Liao, J. Meng, Z. Hao, L. Mai, Carbon-MEMS-based alternating stacked MoS_2@rGO-CNT micro-supercapacitor with high capacitance and energy density. Small (2017). https://doi.org/10.1002/smll.201700639
5. C. Xiang, M. Li, M. Zhi, A. Manivannan, N. Wu, Reduced graphene oxide/titanium dioxide composites for supercapacitor electrodes: shape and coupling effects. J. Mater.Chem. **22**, 19161–19167 (2012). https://doi.org/10.1039/c2jm33177b
6. B. Zhao, T. Wang, L. Jiang, K. Zhang, M.M.F. Yuen, J.-B. Xu, X.Z. Fu, R. Sun, C.-P. Wong, NiO mesoporous nanowalls grown on RGO coated nickel foam as high performance electrodes for supercapacitors and biosensors. Electrochim. Acta **192**, 205–215 (2016). https://doi.org/10.1016/j.electacta.2016.01.211
7. S. Yang, Y. Liu, Y. Hao, X. Yang, W.A. Goddard, X.L. Zhang, B. Cao, Oxygen-vacancy abundant ultrafine Co_3O_4/graphene composites for high-rate supercapacitor electrodes. Adv. Sci. **5**, 1700659 (2018). https://doi.org/10.1002/advs.201700659
8. H. Yang, S. Kannappan, A.S. Pandian, J.-H. Jang, Y.S. Lee, W. Lu, Graphene supercapacitor with both high power and energy density. Nanotechnology **28**, 445401 (2017). https://doi.org/10.1088/1361-6528/aa8948
9. S. Mouri, W. Zhang, D. Kozawa, Y. Miyauchi, G. Eda, K. Matsuda, Thermal dissociation of inter-layer excitons in MoS_2/$MoSe_2$ hetero-bilayers. Nanoscale **9**, 6674–6679 (2017). https://doi.org/10.1039/c7nr01598d
10. J. Luo, P. Xu, D. Zhang, L. Wei, D. Zhou, W. Xu, J. Li, D. Yuan, Synthesis of 3D-MoO_2 microsphere supported $MoSe_2$ as an efficient electrocatalyst for hydrogen evolution reaction. Nanotechnology **28**, 465404 (2017). https://doi.org/10.1088/1361-6528/aa8947
11. B. Zheng, Y. Chen, F. Qi, X. Wang, W. Zhang, Y. Li, X. Li, 3D-hierarchical $MoSe_2$ nanoarchitecture as a highly efficient electrocatalyst for hydrogen evolution. 2D Mater. **4**, 025092 (2017). https://doi.org/10.1088/2053-1583/aa6e65
12. S. Mao, Z. Wen, S. Ci, X. Guo, K.K. Ostrikov, J. Chen, Perpendicularly oriented $MoSe_2$/graphene nanosheets as advanced electrocatalysts for hydrogen evolution. Small **11**, 414–419 (2015). https://doi.org/10.1002/smll.201401598
13. K. Palanisamy, Y. Kim, H. Kim, J.M. Kim, W.S. Yoon, Self-assembled porous MoO_2/graphene microspheres towards high performance anodes for lithium ion batteries. J. Power Sour. **275**, 351–361 (2015). https://doi.org/10.1016/j.jpowsour.2014.11.001
14. H. Tang, K. Dou, C.C. Kaun, Q. Kuang, S. Yang, $MoSe_2$ nanosheets and their graphene hybrids: synthesis, characterization and hydrogen evolution reaction studies. J Mater. Chem. A **2**, 360–364 (2014). https://doi.org/10.1039/c3ta13584e
15. L. Ma, L. Xu, X. Zhou, X. Xu, L. Zhang, Synthesis of a hierarchical $MoSe_2$/C hybrid with enhanced electrochemical performance for supercapacitors. RSC Adv. **6**, 91621–91628 (2016). https://doi.org/10.1039/c6ra16157j
16. S.K. Balasingam, J.S. Lee, Y. Jun, Few-layered $MoSe_2$ nanosheets as an advanced electrode material for supercapacitors. Dalton Trans. **44**, 15491–15498 (2015). https://doi.org/10.1039/c5dt01985k
17. Y.P. Gao, K.J. Huang, H.L. Shuai, L. Liu, Synthesis of sphere-feature molybdenum selenide with enhanced electrochemical performance for supercapacitor. Mater. Lett. **209**, 319–322 (2017). https://doi.org/10.1016/j.matlet.2017.08.044
18. S.S. Karade, B.R. Sankapal, Two dimensional cryptomelane like growth of $MoSe_2$ over MWCNTs: symmetric all-solid-state supercapacitor. J. Electroanal. Chem. **802**, 131–138 (2017). https://doi.org/10.1016/j.jelechem.2017.08.017
19. H. Li, L. Chen, Y. Zhang, X. Ji, S. Chen, H. Song, C. Li, H. Tang, Synthesis of $MoSe_2$/reduced graphene oxide composites with improved tribological properties for oil-based additives. Cryst. Res. Technol. **49**, 204–211 (2014). https://doi.org/10.1002/crat.201300317
20. J. Sha, C. Gao, S.K. Lee, Y. Li, N. Zhao, J.M. Tour, Preparation of three-dimensional graphene foams using powder metallurgy templates. ACS Nano **10**, 1411–1416 (2016). https://doi.org/10.1021/acsnano.5b06857
21. Z. Chen, W. Ren, L. Gao, B. Liu, S. Pei, H.M. Cheng, Three-dimensional flexible and conductive interconnected graphene networks grown by chemical vapour deposition. Nat. Mater. **10**, 424–428 (2011). https://doi.org/10.1038/nmat3001
22. K. Chen, C. Li, Z. Chen, L. Shi, S. Reddy, H. Meng, Q. Ji, Y. Zhang, Z. Liu, Bioinspired synthesis of CVD graphene flakes and graphene-supported molybdenum sulfide catalysts for hydrogen evolution reaction. Nano Res. **9**, 249–259 (2016). https://doi.org/10.1007/s12274-016-1013-1
23. H.J. Qiu, Y. Guan, P. Luo, Y. Wang, Recent advance in fabricating monolithic 3D porous graphene and their applications in biosensing and biofuel cells. Biosens. Bioelectron. **89**, 85–95 (2017). https://doi.org/10.1016/j.bios.2015.12.029
24. S. Mao, G. Lu, J. Chen, Three-dimensional graphene-based composites for energy applications. Nanoscale **7**, 6924–6943 (2015). https://doi.org/10.1039/c4nr06609j
25. H. Bai, C. Li, X. Wang, G. Shi, On the gelation of graphene oxide. J. Phys. Chem. C **115**, 5545–5551 (2011). https://doi.org/10.1021/jp1120299
26. L. Bao, T. Li, S. Chen, C. Peng, L. Li, Q. Xu, Y. Chen, E. Ou, W. Xu 3D Graphene frameworks/Co_3O_4 composites electrode for high-performance supercapacitor and enzymeless glucose detection. Small (2017). https://doi.org/10.1002/smll.201602077
27. E.G. Da Silveira Firmiano, A.C. Rabelo, C.J. Dalmaschio, A.N. Pinheiro, E.C. Pereira, W.H. Schreiner, E.R. Leite, Supercapacitor electrodes obtained by directly bonding 2D MoS_2 on reduced graphene oxide. Adv. Energy Mater. **4**, 1301380 (2014). https://doi.org/10.1002/aenm.201301380
28. K.J. Huang, J.Z. Zhang, Y. Fan, Preparation of layered $MoSe_2$ nanosheets on Ni-foam substrate with enhanced supercapacitor performance. Mater. Lett. **152**, 244–247 (2015). https://doi.org/10.1016/j.matlet.2015.03.130
29. S.K. Balasingam, J.S. Lee, Y. Jun, Molybdenum diselenide/reduced graphene oxide based hybrid nanosheets for supercapacitor applications. Dalton Trans. **45**, 9646–9653 (2016). https://doi.org/10.1039/c6dt00449k

30. J. Chen, B. Yao, C. Li, G. Shi, An improved Hummers method for eco-friendly synthesis of graphene oxide. Carbon **64**, 225–229 (2013). https://doi.org/10.1016/j.carbon.2013.07.055
31. X. Liu, J.Z. Zhang, K.-J. Huang, P. Hao, Net-like molybdenum selenide–acetylene black supported on Ni foam for high-performance supercapacitor electrodes and hydrogen evolution reaction. Chem. Eng. J. **302**, 437–445 (2016). https://doi.org/10.1016/j.cej.2016.05.074
32. Y. Liu, T. Gao, H. Xiao, W. Guo, B. Sun, M. Pei, G. Zhou, One-pot synthesis of rice-like TiO_2/graphene hydrogels as advanced electrodes for supercapacitors and the resulting aerogels as high-efficiency dye adsorbents. Electrochim. Acta **229**, 239–252 (2017). https://doi.org/10.1016/j.electacta.2017.01.142
33. J. Yao, B. Liu, S. Ozden, J. Wu, S. Yang, M.T.F. Rodrigues, K. Kalaga, P. Dong, P. Xiao, Y. Zhang, R. Vajtai, P.M. Ajayan, 3D nanostructured molybdenum diselenide/graphene foam as anodes for long-cycle life lithium-ion batteries. Electrochim. Acta **176**, 103–111 (2015). https://doi.org/10.1016/j.electacta.2015.06.138
34. S. Sankar, A.I. Inamdar, H. Im, S. Lee, D.Y. Kim, Template-free rapid sonochemical synthesis of spherical α-MnO_2 nanoparticles for high-energy supercapacitor electrode. Ceram. Int. **44**, 17514–17521 (2018). https://doi.org/10.1016/j.ceramint.2018.05.207
35. J.K. Jayaramulu, D.P. Dubal, B. Nagar, V. Ranc, O. Tomanec, M. Petr, K.K.R. Datta, R. Zboril, P. Gomez-Romero, R.A. Fischer, Ultrathin hierarchical porous carbon nanosheets for high-performance supercapacitors and redox electrolyte energy storage. Adv. Mater. **30**, 1705789 (2018). https://doi.org/10.1002/adma.201705789
36. J. Zhao, Y. Jiang, H. Fan, M. Liu, O. Zhuo, X. Wang, Q. Wu, L. Yang, Y. Ma, Z. Hu, Porous 3D few-layer graphene-like carbon forultrahigh-power supercapacitors with well-defined structure-performance relationship. Adv. Mater. **29**, 1604569 (2017). https://doi.org/10.1002/adma.201604569
37. X. Gao, H. Yue, E. Guo, L. Yao, X. Lin, B. Wang, E. Guan, D. Bychanok, In-situ polymerization growth of polyaniline nanowire arrays on graphene foam for high specific capacitance supercapacitor electrode. J Mater. Sci. Mater. Electron. **28**, 17939–17947 (2017). https://doi.org/10.1007/s10854-017-7736-2
38. S. Ahmed, M. Rafat, Hydrothermal synthesis of PEDOT/rGO composite for supercapacitor applications. Mater. Res. Express (2017) https://doi.org/10.1088/2053-1591/aaa232
39. S. Ahmed, M. Rafat, Effect of lithium and sodium salt on the performance of Nb_2O_5/rGO nanocomposite based supercapacitor. Mater. Res. Express (2018). https://doi.org/10.1088/2053-1591/aaace2
40. A. Sultan, R. Mohd, M.K. Singh, S. Hashmi, A Free-standing, flexible PEDOT-PSS film and its nanocomposites with graphene nano-platelets as electrodes for quasi-solid-state supercapacitors. Nanotechnology (2018). https://doi.org/10.1088/1361-6528/aad0b8
41. Y. Yang, F. Huilong, R. Gedeng, X. Changsheng, J.M. Tour, Edge-oriented MoS_2 nanoporous films as flexible electrodes for hydrogen evolution reactions and supercapacitor devices. Adv. Mater. **26**, 8163–8168 (2014). https://doi.org/10.1002/adma.201402847
42. W. Lu, M. Arif, G. Duan, S. Chen, X. Liu, A high performance quasi-solid-state supercapacitor based on $CuMnO_2$ nanoparticles. J. Power Sour. **355**, 53–61 (2017). https://doi.org/10.1016/j.jpowsour.2017.04.054
43. P. Hui, J. Zhou, K. Sun, G. Ma, Z. Zhang, E. Feng, Z. Lei, High-performance asymmetric supercapacitor designed with a novel NiSe@$MoSe_2$ nanosheet arrays and nitrogen-doped carbon nanosheet. Acs Sustaina Chem Eng **5**, 59514–59563 (2017). https://doi.org/10.1021/acssuschemeng.7b00729
44. S.N. Tiruneh, B. Kang, S.H. Kwag, Y.H. Lee, M.S. Kim, D.H. Yoon, Synergistically active $NiCo_2S_4$ nanoparticles coupled with holey defect graphene hydrogel for high-performance solid-state supercapacitors. Chem. Eur. J. **24**, 3263–3270 (2018). https://doi.org/10.1002/chem.201705445
45. K. Ghosh, C.Y. Yue, Development of 3D MoO_3/graphene aerogel and sandwich-type polyaniline decorated porous MnO_2-graphene hybrid film based high performance all-solid-state asymmetric supercapacitors. Electrochim. Acta **276**, 47–63 (2018). https://doi.org/10.1016/j.electacta.2018.04.16